Available online at www.sciencedirect.com

SciVerse ScienceDirect

Ceramics International 39 (2013) 3049–3054

CERAMICS INTERNATIONAL

www.elsevier.com/locate/ceramint

Corrosion of aluminum oxynitride based ceramics by molten steel

X.J. Zhao[a], H.Q. Ru[a,*], N. Zhang[b], X.Y. Wang[a,b], D.L. Chen[c]

[a]Department of Materials Science and Engineering, School of Materials and Metallurgy, Northeastern University, Shenyang, Liaoning 110004, China
[b]Key Laboratory of Advanced Materials Manufacturing Technology of Liaoning Province, Shenyang University, Shenyang, Liaoning 110044, China
[c]Department of Mechanical and Industrial Engineering, Ryerson University, Toronto, Ontario, Canada M5B 2K3

Received 20 August 2012; received in revised form 25 September 2012; accepted 25 September 2012
Available online 7 October 2012

Abstract

Aluminum oxynitride (AlON) exhibits excellent stability, chemical and mechanical properties. Corrosion resistance to molten steel is an important performance index of ceramic refractories. While silicon carbide (SiC) particles have been proven to improve the mechanical properties and thermal shock resistance of AlON ceramic, the corrosion of AlON and SiC–AlON composites by molten steel were unknown. The aim of this investigation was to evaluate the corrosion resistance to molten steel and identify the underlying mechanisms of AlON ceramic and 8 wt% SiC–AlON composites at the temperature of 1550 °C for 30 min. Due to the reaction between AlON and molten steel, a solid product of Al_2O_3 is detected in the corrosion region. Besides, some round shaped pores form and increase toward the sample surface in the corrosion region. The thickness of corrosion region of AlON ceramic is about 150 μm, indicating that the AlON ceramic has an excellent corrosion resistance to molten steel. However, the corrosion resistance of 8 wt% SiC–AlON composites to molten steel can be characterized with a penetrated depth of approximately 250 μm. This is mainly attributed to the thermal dissociation of SiC and the reaction between SiC and molten steel.

Keywords: AlON; SiC; Corrosion; Molten steel

1. Introduction

Refractory degradation is a complex phenomenon involving chemical wear (corrosion) and physical/mechanical wear (erosion/abrasion). Refractory corrosion results in the recession of hot face (working surface) due to chemical reaction and molten metal penetration [1,2]. Corrosion resistance to molten steel is one of the major issues for ultra-high temperature ceramics to be used in the refractory industries. Recently, due to the rapidly increased demands of advanced ceramics in the metallurgical industry, lots of studies have paid attention to their corrosion behavior [3,4].

As a solid solution of Al_2O_3 and AlN [5], aluminum oxynitride ($Al_{2.81}O_{3.56}N_{0.44}$) can be used in steelmaking applications owing to its excellent high-temperature mechanical and chemical properties such as high rigidity and good chemical stability [6,7]. Furthermore, AlON particles have been demonstrated to be able to improve the high-temperature mechanical properties and friction resistance of Al_2O_3 matrix ceramic against steel [8,9].

Silicon carbide (SiC) has been reported to be an important structural ceramic due to good mechanical and thermal properties. SiC ceramic exhibits good wear, creep and oxidation resistance at high temperatures [10,11]. It has been shown that the SiC particles could effectively improve the mechanical properties [9,12], oxidation behavior [13] and thermal shock behavior [14] of AlON ceramic. However, to the authors' knowledge, there is little information in the open literature regarding the corrosion resistance of AlON ceramic and SiC–AlON composites to molten steel. The questions remain unanswered over how high the corrosion resistance of AlON ceramic to molten steel is, if and to what extent the nano-sized SiC particles can affect the corrosion resistance of AlON ceramic. Therefore, in this paper, the corrosion resistance of AlON ceramic and SiC–AlON composites to molten steel was evaluated and analyzed, with special

*Corresponding author. Tel./fax: +86 024 83680248
E-mail address: ruhq@smm.neu.edu.cn (H.Q. Ru).

0272-8842/$ - see front matter © 2012 Elsevier Ltd and Techna Group S.r.l. All rights reserved.
http://dx.doi.org/10.1016/j.ceramint.2012.09.084

attention to the influence of nano-sized SiC particles on the corrosion resistance of SiC–AlON composites.

2. Experimental procedure

2.1. Preparation of samples

In the present study, β-SiC (40–90 nm, Nanjing Emperor Nano-Material Co., Ltd., China, 99.5%) powders and AlON powders which were prepared by Al_2O_3 (40–100 nm, Nanjing Emperor Nano-Material Co., Ltd., China, 99.5%) and AlN (30–100 nm, Shenzhen Honesty Nano-Tech Co., Ltd., China, 99%) were used as raw materials. Due to its superior mechanical properties and oxidation behavior, 8 wt% SiC–AlON ceramic composite was prepared. Firstly, 8 wt% nano-sized SiC particles were added into AlON powders and thoroughly mixed. Secondly, the mixed powders were attrition milled for 24 h using ethanol as a milling medium and dried at 80 °C. Thirdly, the dried SiC–AlON powders were crushed using mortar and then sieved through a 180 μm mesh. Finally, both pure AlON powders and the sieved powders were put in the graphite dies and sintered at 1850 °C under a pressure of 25 MPa for 40 min in nitrogen atmosphere. The heating rate was 10 °C/min below 1400 °C and then adjusted as 5 °C/min between 1400 °C and 1850 °C. Finally, the sintered AlON ceramic and SiC–AlON composites were cooled down to the room temperature in the furnace.

2.2. Characterization

The microstructures of the raw powders and the cross-section of the specimen were examined using scanning electron microscope (SEM). To achieve a better resolution on the SEM images, the specimens were sputter-coated with a thin film of gold. The phase and crystallinity were analyzed via X-ray diffraction (XRD) using CuK_α radiation at 45 kV and 40 mA. The diffraction angle (2θ) at which the X-rays hit the sample varied from 10° to 90° with a step size of 0.05° and 1 s in each step.

2.3. Corrosion experiments

The corrosion test specimens of AlON and 8 wt% SiC–AlON, with a diameter of 43 mm, were ground and polished to a surface finished using 1 μm diamond paste. To avoid being blown away during air exhaust or inflate, Fe powders were pressed into tablets with a diameter of 13 mm in a steel die under a pressure of 250 MPa at room temperature. Initially, the corrosion specimens were put into a horizontal tube furnace and the Fe tablets were put on the middle of the substrates; then, the AlON and SiC–AlON ceramics as well as Fe tablets were heat treated at 1550 °C for 30 min under nitrogen atmosphere. After cooling, all the cross-sections of the corroded specimens were prepared by cutting perpendicularly to the interfaces. All specimens were sectioned and polished to a surface finished using 1 μm diamond paste for microstructural investigations. Finally, the microstructural features of the ceramic materials after the corrosion tests were analyzed by SEM. Before SEM analysis, the polished specimens were coated with gold to improve the conductivity of the specimens. Energy dispersive spectroscopy (EDS) was used to identify the elemental distribution in the selected region.

3. Results

The XRD patterns of pure AlON and 8 wt% SiC–AlON composites have been reported in our previous work [14]. No other new phases or impurities were identified in both patterns of either sintered AlON or SiC–AlON composites.

3.1. Microstructure of raw powders and sintered ceramic

Fig. 1 shows the SEM micrographs of the prepared AlON powders and β-SiC powders. It is seen from Fig. 1(a) that the spinel-type structure of prepared AlON powders is similar to that reported in [5,15]. The AlON powders have an average size of about 4 μm. Fig. 1(b) shows that most of SiC particles are nano-sized (< 100 nm) with a conglomeration. In sample preparation for SEM measurements, it is normally difficult to disperse nano-sized particles on a copper plate even though after ultrasonic vibration.

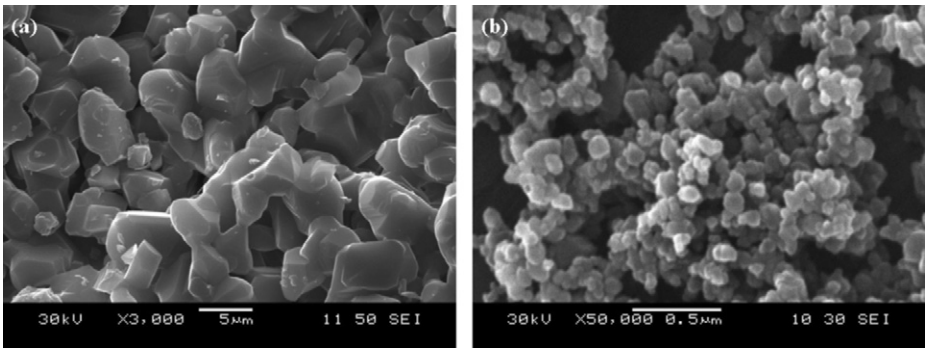

Fig. 1. SEM micrographs of raw powders for (a) AlON powders and (b) nano-sized SiC powders.

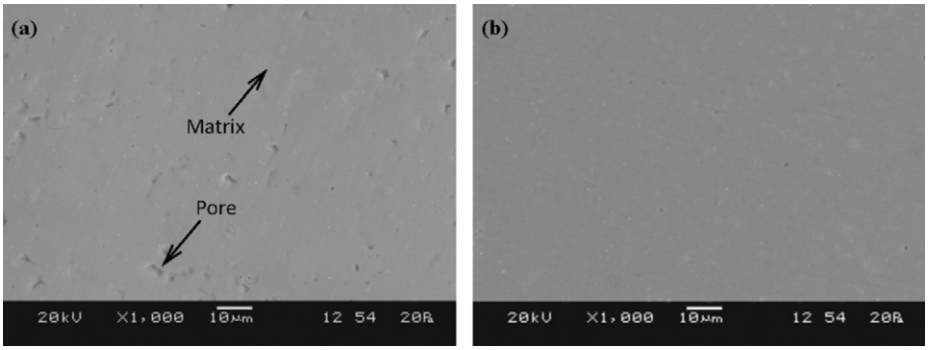

Fig. 2. SEM micrographs from the polished specimen surfaces of the synthesized (a) pure AlON and (b) 8 wt%SiC–AlON composites.

Fig. 2 shows typical SEM micrographs of AlON and 8 wt%SiC–AlON composites. From Fig. 2(a), it is seen that a great number of pores homogeneously disperse in the surface of pure AlON. Fig. 2(b) shows that with 8 wt% SiC particles addition the quantity of pores decrease considerably. In other words, the SiC–AlON composite is denser than pure AlON. However, it is very difficult to observe the SiC particles from the polished specimen surface (Fig. 2(b)). This is attributed to the fact that the colors between AlON matrix and SiC are very similar under SEM. It is in agreement with the results reported in our recent publication [12] that the relative densities of AlON and 8 wt% SiC–AlON are 97.6% and 99.6%, respectively.

3.2. Change in the microstructure after corrosion tests

Fig. 3 shows the microstructure and EDS results from the cross section of the corroded AlON ceramic. After heat-treatment at 1550 °C in nitrogen atmosphere for 30 min, the white corrosion products can be observed near the specimen surface. Meanwhile, a boundary appeared between the white region and the inner AlON matrix as shown in Fig. 3(a) and (b). Then, it is seen that the region in the section of AlON ceramic without corrosion in molten steel did not exhibit an obvious change, with a surface layer of about 10–20 μm in the specimen (Fig. 3(a)). However, a corrosion layer of about 150 μm in the corroded region of AlON ceramic in molten steel observed as shown in Fig. 3(b). As shown in Fig. 3(c) and (d), it can be found that the oxygen is considerably higher and the aluminum is lower in the corrosion region than these in the inner AlON matrix. It suggests that amount of Al_2O_3 are formed in the corroded region during molten steel corrosion experiments. This would be attributed to the corroding effects of the molten steel. The details will be presented in the discussion section. SEM micrographs with a high magnification ($\times 1000$) of corrosion region and AlON matrix taken from the cross section of AlON specimen corroded by molten steel are shown in Fig. 3(e) and (f), respectively. Additionally, it should be noted that the white corrosion layer was partially gone during cutting, grinding and polishing even though each sample was clamped using an aluminum holder to protect the surface layer. This is mainly due to the looseness of the corroded products, as shown in Fig. 3(b) and (e).

Fig. 4 shows the microstructure and EDS results taken from the cross section of the corroded specimen of 8 wt% SiC–AlON ceramic. After heat-treatment at 1550 °C in nitrogen atmosphere for 30 min, the similar microstructural morphologies as AlON ceramic are observed, and a boundary between the white layer and the inner AlON matrix appeared as shown in Fig. 4(a) and (b). The non-corroded section of the SiC–AlON specimen had no significant change either, with a surface layer of about 20 μm (Fig. 4(a)). However, in the corroded section of the SiC–AlON specimen by molten steel, the corrosion region of SiC–AlON specimen became thicker and it was about 250 μm (Fig. 4(b)). Furthermore, it was found that some products with ball shape appeared in the corrosion region as shown in Fig. 4(b). The EDS results show that the content of Fe is remarkably high in the ball shaped products. It is certificated that the ball products are cooled molten-steel that penetrate into the SiC–AlON specimens during the specimen heat-treatment at 1550 °C for 30 min. This would be attributed to the presence of SiC and molten steel. The details will be presented in the discussion section. Additionally, it can also be seen from Fig. 4(a) and (b) that the non-corroded region of the sample (at the lower portion of the images) is very dense which matches well with the measured relative density of more than 99%.

4. Discussion

For engineering application of AlON-based ceramics in steel industry, the knowledge of corrosion resistance to molten steel is very important. Thus, the corrosion resistance to molten steel has become an important performance index to evaluate AlON-based ceramic materials in these applications.

4.1. Corrosion behavior of AlON ceramic

The cross section of AlON specimen corroded by molten steel can be divided into two regions as shown in Fig. 3(a) and (b). In comparison with Fig. 3(a), the microstructure

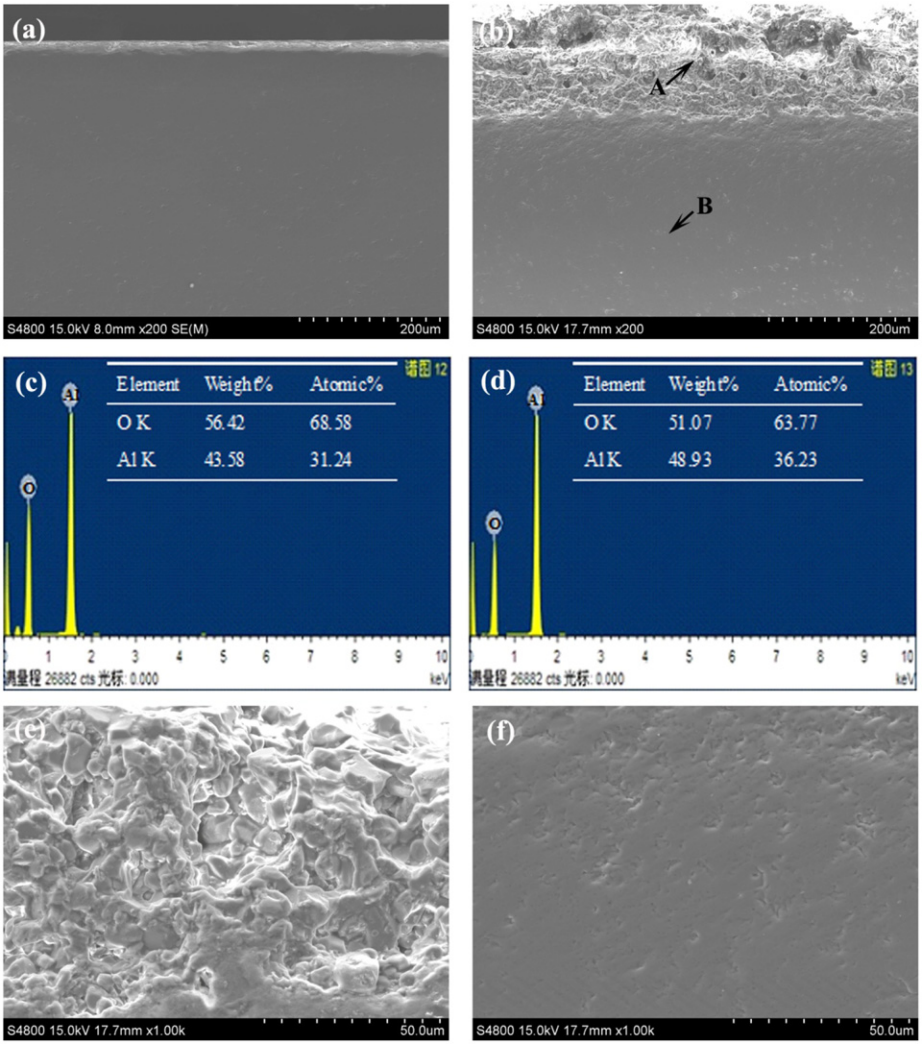

Fig. 3. SEM micrographs from the cross section of AlON specimen corroded by molten steel: (a) non-corroded area; (b) corroded area; (c) EDS for point A; (d) EDS for point B; (e) corrosion region and (f) inner AlON matrix.

as shown in Fig. 3(b) indicated that the molten steel played a significant role in the thickness of corrosion region of AlON specimen. After heat-treatment at 1550 °C for 30 min, the thickness of surface layer in non-corroded area by molten steel is about 20 μm (Fig. 3(a)). However, the corrosion region by molten steel is observed in AlON ceramic with a thickness of 150 μm as shown in Fig. 3(b). The thickness for molten steel corroded section is obviously higher compared to non-corroded section in the AlON ceramic. This is mainly attributed to the reaction between AlON and molten steel. The corrosion resistance of AlON refractory is influenced by its reactions with molten steel, which leads to the dissolution of refractory constituents into the melt. Thus, it is evident that the thickness of corrosion region remarkably increased with molten steel penetrated into the AlON refractory.

Then, the corrosion of AlON refractory is primarily influenced by its chemical reactions with molten steel, which proceed through a direct contact with the metal [2]. The reaction between AlON and molten steel produced Al_2O_3 as solid products as seen from the EDS results of Fig. 3(d). Meanwhile, in the graphite resistance furnace and graphite crucible, some gaseous species like Al_2O, CO and N_2 were also generated due to the presence of carbon in the reaction system [4]. Besides, the pores size increased toward the surface of the AlON specimen. The formation of gaseous species decreased the density of corrosion region and could be documented by the round shaped pores as shown in Fig. 3(b) and (e). A similar result was also reported in β-Sialon based ceramic [4].

Besides, refractory-steel reactions lead to molten metal penetration. The penetration depth is believed to be influenced by the chemical composition of the refractory, metal and physical properties such as porosity of the refractory. To some extent, high metal penetration into ceramic refractories can be caused by the high porosity of the refractory. In present study, due to fully dense of AlON ceramic, molten steel is difficult to penetrate into the AlON refractory and low penetration of AlON samples is observed in Fig. 3(b). As mentioned above, the corrosion

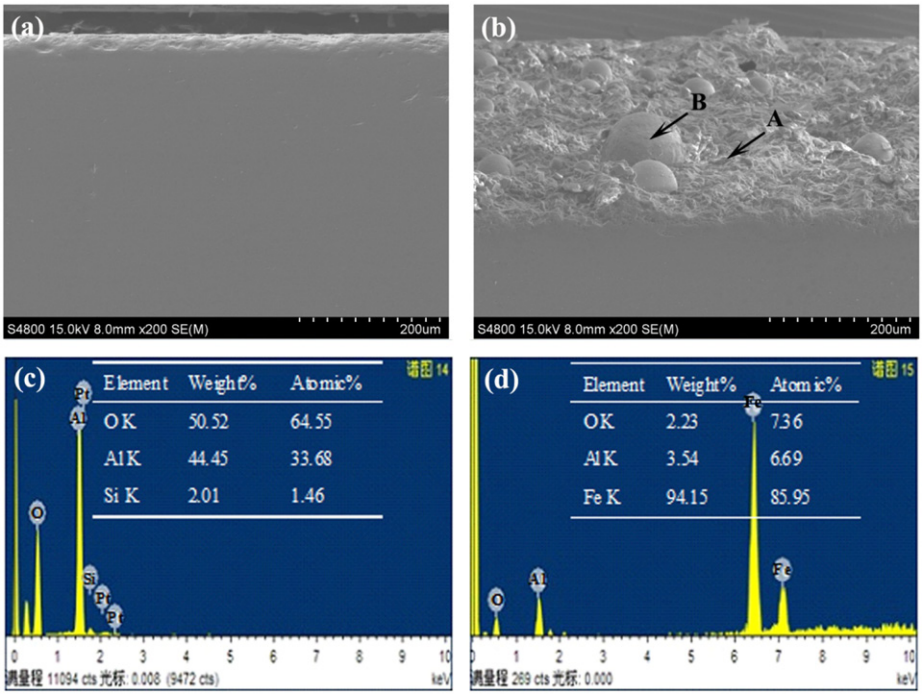

Fig. 4. SEM micrographs from the cross section of SiC–AlON composites corroded by molten steel: (a) non-corroded area; (b) corroded area; (c) EDS for point A and (d) EDS for point B.

region with just about 150 μm by molten steel is characterized for the dense AlON ceramic as shown in Fig. 3(b) and (e). However, it was reported that with 10% carbon adding into alumina ceramic, although carbon in the form of graphite could be used to enhance the corrosion resistance and thermal shock resistance of alumina ceramic refractories [2,16], a corrosion region of 290–320 μm was observed in the similar corrosion conditions as the present study (heat-treatment at 1550 °C for 30 min) [2]. Thus, these show that the AlON ceramic has an excellent corrosion resistance to molten steel.

Additionally, it should be pointed out that the element of Fe is not detected in the corrosion layer of AlON specimen as seen in Fig. 3(c). This could be attributed to the following two possible reasons: firstly, due to the excellent corrosion resistance of AlON, the content of penetrated molten steel is limited and secondly, due to the weak interface force between AlON or Al_2O_3 and Fe, the molten steel is easy to be gone from the cross section surface of AlON specimen during cutting, grinding and polishing.

4.2. Corrosion behavior of SiC–AlON composites

It is similar as AlON ceramic that the molten steel is observed to penetrate deep into the SiC–AlON specimen. Furthermore, it is interesting to perceive that the porosity increased toward the surface of the SiC–AlON specimen.

On one hand, it can be seen from Fig. 4(d) that, in the corrosion region of SiC–AlON specimen, the melt spheroids of steel are formed. This probably as a result of the corrosion reactions could be attributed to the enhanced penetration of molten steel and the wettability behavior by adding SiC particles in AlON matrix. However, it should be pointed out that the element of Si is not detected in melt spheroids of steel as seen in Fig. 4(d). It could be attributed to the following two possible reasons: first, the wt% of Si in AlON is limited. Furthermore, the atomic weight of Si is lighter than Fe, thus it is difficult to be detected in the molten steel. Second, during the cooling process of the SiC–AlON specimen after corrosion by molten steel, the cooling rates of Si and Fe are different, and the Si is easily nucleating in the inner of molten steel. Only the elements in the surface of the molten steel can therefore be detected by the EDS.

On the other hand, the interfacial behavior of SiC–AlON composites revealed significantly higher molten steel penetration compared to AlON ceramic. As mentioned above, the penetration depth of molten steel in AlON composites is about 150 μm (Fig. 3(b)). Nevertheless, the refractory matrix and interfacial region of SiC–AlON composites show that the molten steel has penetrated by a depth of approximately 250 μm as seen in Fig. 4(b). The increase in the thickness of corrosion region observed during the experimentation must be assigned to the thermal dissociation of SiC in molten steel. It is occurred by the dissolution of the resulting elements in the liquid phase via the following reaction [17,18]:

$$SiC_{(specimen)} \rightarrow [Si]_{steel} + [C]_{steel} \quad (1)$$

Such a thermal dissociation of SiC and the reaction between SiC and molten steel could speed the inward penetration of molten steel through the corrosion region, thus considerably reduce the corrosion resistance to molten

steel. Meanwhile, the partly position of SiC particles after corrosion tests would be replaced by the round shaped pores. As reported, material inhomogeneity and porosity could promote corrosion and allow corrosive agents to penetrate and cause erosive damage, resulting in severe degradation [19,20]. Thus, it is clear that the molten steel penetration increased with the addition of nano-sized SiC particles in the AlON refractory.

Based on the above results and discussion, it can be concluded that the AlON ceramic has an excellent corrosion resistance to molten steel while the addition of 8 wt% SiC in the AlON matrix compromises it. More studies are needed to further improve and optimize the corrosion resistance of AlON ceramic.

5. Conclusions

The corrosion resistance to molten steel of aluminum oxynitride (AlON) and 8 wt% SiC–AlON composites with a relative density of 97% were investigated by means of heat treating at a temperature of 1550 °C for 30 min under nitrogen atmosphere. The molten steel played a significant role in the thickness of corrosion region of both AlON and SiC–AlON specimens. It was observed that the cross sections of the specimens corroded by molten steel could be divided into two regions. The reaction between AlON and molten steel produced Al_2O_3 as solid products in the corrosion region. Additionally, some gaseous species were also generated due to the presence of carbon in the reaction system. And the pores number and size increased toward the surface of the specimen. The corrosion region in molten steel was observed to exist in AlON ceramic with a thickness of about 150 μm, indicating AlON ceramic has an excellent corrosion resistance to molten steel. However, the addition of 8 wt% SiC in the AlON matrix led to an increase in the penetration depth of molten steel with a corroded region of about 250 μm due to the thermal dissociation of SiC and the reaction between SiC and molten steel.

Acknowledgments

The authors would like to thank the financial support of the National Natural Science Foundation of China (NSFC Grant Nos. 51072121 and 50672060) and the Natural Sciences and Engineering Research Council of Canada (NSERC) in the form of international research collaboration. D.L. Chen is also grateful for the financial support by NSERC-DAS Award, Premier's Research Excellence Award (PREA), Canada Foundation for Innovation (CFI), and Ryerson Research Chair (RRC) program. The authors would also like to thank Professor X.D. Sun (Northeastern University) for the helpful discussion and suggestion, and H.M. Kan (Shenyang University), Q. Li, A. Machin, J. Amankrah and R. Churaman (Ryerson University), for their assistance in the experiments. X.J. Zhao as an international exchange Ph.D. student also gratefully acknowledges the financial support provided by China Scholarship Council.

References

[1] S.C. Carniglia, G.L. Barna, Handbook of Industrial Refractories Technology: Principles, Types, Properties and Applications, Noyes Publications, New Jersey, 1992, pp. 67–132.
[2] M. Ikarm-ul-Haq, R. Khanna, P. Koshy, V. Sahajwalla, High-temperature interactions of alumina-carbon refractories with molten iron, ISIJ International 50 (2010) 804–812.
[3] F.L. Riley, The corrosion of ceramics: where do we go from here?, Key Engineering Materials 113 (1996) 1–14
[4] J. Krestan, O. Pritula, L. Smrcok, P. Sajgalik, Z. Lences, A. Wannberg, F. Monteverde, Corrosion of β-Sialon-based ceramics by molten steel, Journal of the European Ceramic Society 27 (2007) 2137–2143.
[5] N.D. Corbin, Aluminum oxynitride spinel: a review, Journal of the European Ceramic Society 5 (1989) 143–154.
[6] X.D. Wang, F.M. Wang, W.C. Li, Synthesis, microstructures and properties of γ-aluminum oxynitride, Materials Science and Engineering A 342 (2003) 245–250.
[7] J. Zheng, B. Forslund, Carbothermal synthesis of aluminium oxynitride (AlON) powder: influence of starting materials and synthesis parameters, Journal of the European Ceramic Society 15 (1995) 1087–1100.
[8] D. Goeuriot-Launay, F. Goeuriot, F. Thevenot, G. Orange, G. Fantozzi, R. Trabelsi, D. Treheux, Effect of γ-aluminium oxynitride dispersion on some alumina properties, Ceramics International 15 (1989) 207–212.
[9] D. Djenkal, D. Goeuriot, F. Thevenot, SiC-reinforcement of an Al_2O_3–γAlON composite, Journal of the European Ceramic Society 20 (2000) 2585–2590.
[10] A. Kovalcikova, J. Dusza, P. Sajgalik, Thermal shock resistance and fracture toughness of liquid-phase-sintered SiC-based ceramics, Journal of the European Ceramic Society 29 (2009) 2387–2394.
[11] K. Yamada, N. Kamiya, High temperature mechanical properties of Si_3N_4–$MoSi_2$ and Si_3N_4–SiC composites with network structures of second phases, Materials Science and Engineering A 261 (1999) 270–277.
[12] X.J. Zhao, N. Zhang, H.Q. Ru, B. Liang, D.L. Chen, Mechnical properties and toughening mechanisms of silicon carbide nano-particulate reinforced AlON composites, Materials Science and Engineering A 538 (2012) 118–124.
[13] X.J. Zhao, D.L. Chen, H.Q. Ru, N. Zhang, B. Liang, Oxidation behabiour of nano-sized SiC particulate reinforced AlON composites, Journal of the European Ceramic Society 31 (2011) 2255–2265.
[14] X.J. Zhao, H.Q. Ru, D.L. Chen, N. Zhang, B. Liang, Thermal shock behavior of nano-sized SiC particulate reinforced AlON composites, Materials Science and Engineering B 177 (2012) 402–410.
[15] X.J. Zhao, D.L. Chen, H.Q. Ru, N. Zhang, Zirconium nitride nano-particulate reinforced AlON composites: fabrication, mechanical properties and toughening mechanisms, Journal of the European Ceramic Society 31 (2011) 883–892.
[16] R. Khanna, V. Sahajwalla, B. Rodgers, F. McCarthy, Dissolution of carbon from alumina–carbon mixtures into liquid iron: influence of carbonaceous materials, Metallurgical and Materials Transactions B 37 (2006) 623–632.
[17] A.A. Amadeh, J.C. Labbe, P.E. Quintard, Behaviour of the wettability of a SiAlON-base ceramic by molten steel, Journal of the European Ceramic Society 25 (2005) 1041–1048.
[18] S. Kalogeropoulou, L. Baud, N. Eustathopoulos, Relationship between wettability and reactivity in Fe/SiC system, Acta Metallurgica et Materialia 43 (1995) 907–912.
[19] L. Bradley, L. Li, H.F. Stott, Characteristics of the microstructures of alumina-based refractory materials treated with CO_2 and diode lasers, Applied Surface Science 138–139 (1999) 233–239.
[20] J.J. Petrovic, A.K. Vasudevan, Key developments in high temperature structural silicides, Materials Science and Engineering A 261 (1999) 1–5.